CHEMCATCHEM

Supporting Information

Irradiation Direction-Dependent Surface Charge Recombination in Hematite Thin-Film Oxygen Evolution Photoanodes

Guancai Xie[+], Xiaoyue Zhang[+], Xiao Ouyang[+], Qi Xin, Beidou Guo,* and Jian Ru Gong*This manuscript is part of the Special Issue “Photocatalysis: From Solar Power to Sustainable Chemical Production”, which is part of the wider project “Building A New Energy Economy with Catalysis”.

Supporting Information

Irradiation Direction-dependent Surface Charge Recombination in Hematite Thin-film Oxygen Evolution Photoanodes

Guancai Xie, [†] [a, b] Xiaoyue Zhang, [†] [c] Xiao Ouyang, [†] [a, b] Qi Xin,[a] Beidou Guo, * [a, b] and Jian Ru Gong*[a]

[a] G. Xie, X. Zhang, X. Ouyang, Prof. Q. Xin, B. Guo, Prof. J. R. Gong
Chinese Academy of Sciences (CAS) Key Laboratory of Nanosystem and Hierarchy Fabrication, CAS Center for Excellence in Nanoscience
National Center for Nanoscience and Technology
Beijing 100190 (China)
E-mail: guobd@nanoctr.cn; gongjr@nanoctr.cn

[b] G. Xie, X. Ouyang, B. Guo
University of Chinese Academy of Sciences
Beijing 100049 (China)

[c] X. Zhang
School of Materials and Energy
Southwest University
Chongqing 400715 (China)

†These authors contributed equally.

Supplemental Note 1: Synthesis of single layer polystyrene microsphere template

0.1g of polystyrene microsphere with a 600 nm diameter, which was synthesized following the method reported in the reference [1],[1] was dissolved in 2 ml of an ethanol/water solution with an ethanol/water volume ratio of 1:1, and sonicated for 1 hour to get the polystyrene microsphere solution. Pre-cleaned ITO substrates and Si wafer were incubated at 75°C in a hydrophilic solution containing ammonia, hydrogen peroxide, and deionized water with a volume ratio of 1:1:5 for 1 hour. Then, the polystyrene microsphere solution was dropped on the silicon wafer using a 1 mL syringe, and made it spread slowly along the silicon wafer to the deionized water (containing 100 ul of 2% sodium lauryl sulfate as the active agent) in a Petri dish. The polystyrene microspheres would self-assemble on the surface of the water in the Petri dish as a monolayer membrane. Finally, the cleaned ITO was slowly moved under the monolayer film of the polystyrene microsphere, and slowly picked up. After drying naturally, the ITO substrates covered by closely packed monolayer of polystyrene microspheres template can be obtained.

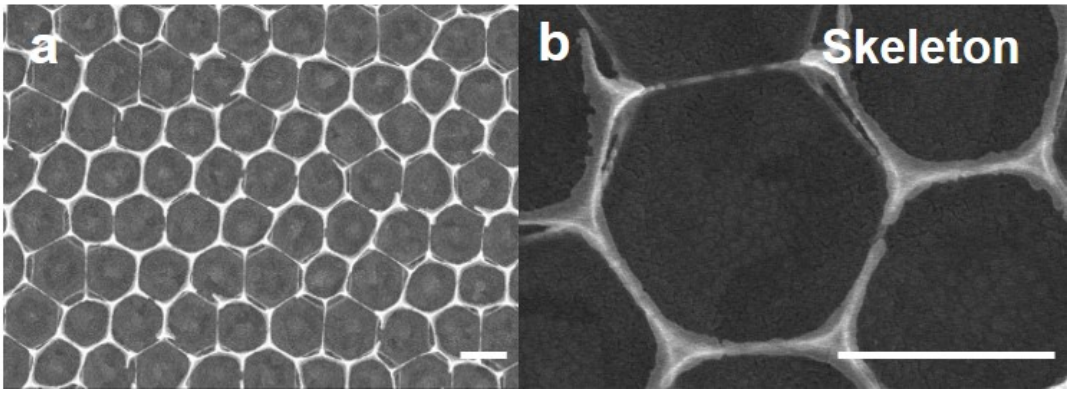

Figure S1. The SEM images of α-Fe_2O_3 skeleton. The scale bar is 500 nm.

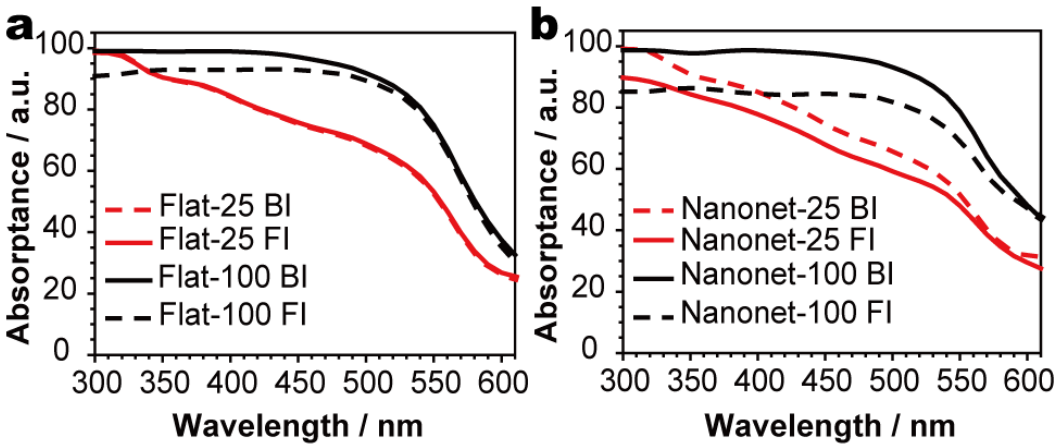

Figure S2. UV-visible absorption spectra of (a) Flat and (b) Nanonet hematite photoanodes with different thicknesses under frontside irradiation and backside irradiation.

The absorption of the Flat-25 sample under frontside and backside irradiation is very close. In the 300-550 nm wavelength range, the Flat-100 samples exhibit higher absorption in the backside irradiaiton mode because the frontside irradiaiton mode resulting in increased diffuse reflection of light in this band. In the 350-550 nm wavelength range, thick sample exhibits stronger light absorption than thin sample, regardless of frontside or backside irradiation, due to the reduced transmission of light with thickening of the planar hematite film. In general, the absorption of planar hematite photoanodes under frontside irradiation is weaker than that under backside irradiation, especially for thick samples, which is the result of diffuse reflection of the surface of the planar hematite larger than the surface of the substrate. And the introduction of nanonet structure has little effect with different irradiation directions on light absorption compared to flat films for the same thickness. The light absorption for the 100 nm thickness of nanonet photoanode is even smaller than that of the 100 nm thickness of planar photoanode under frontside irradiation. It can be also inferred that the Flat samples have higher light absorption under frontside irradiation than the Nanonet samples. This phenomenon can be explained by the high light reflectance resulting from the enhanced light scattering of the surface nanonet structure in Nanonet samples, as can be observed from their reflectance spectra in Figure S3.

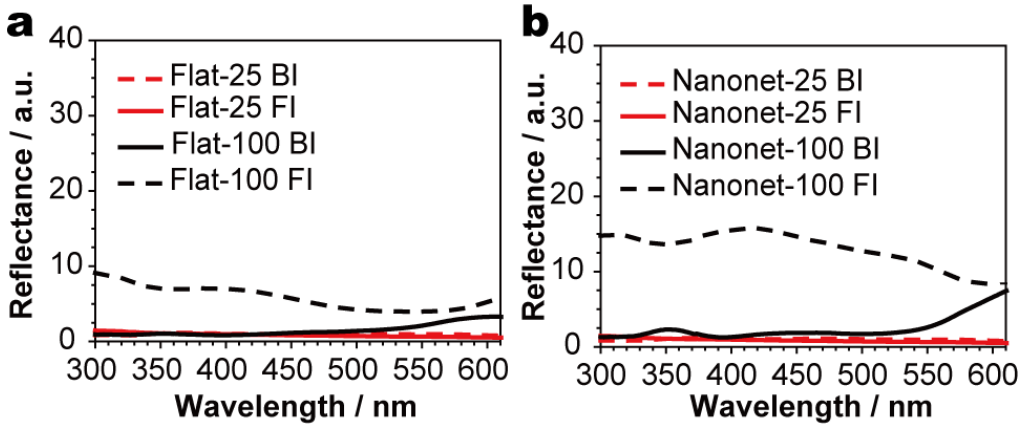

Figure S3. UV-visible reflectance spectra of (a) Flat and (b) Nanonet hematite photoanodes with different thicknesses under frontside irradiation and backside irradiation.

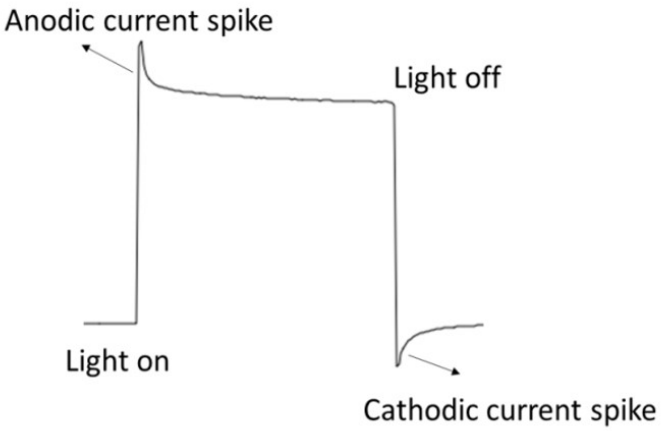

Figure S4. Anodic current spike and cathodic current spike schematic diagram in a photoanode.

As shown in Figure S4, in a photoanode, an anodic photocurrent spike is generated during the switching of the electrode from a dark state to a light, corresponding to the equilibrium process in which photogenerated holes accumulate at the SCLJ and gradually recombines with photogenerated electrons.

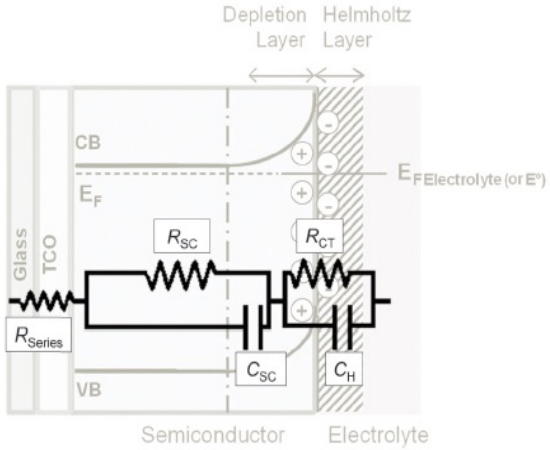

Figure S5. The equivalent circuit used for PEIS data fitting.[5]

R_{CT} represents the charge transfer resistance of the semiconductor/solution interface; C_H represents the capacitance of the Helmholtz layer; R_{sc} represents the bulk electron transport resistance; C_{sc} represents the space charge layer capacitance; and R_s (R_{series}) other series resistance in the system.

Table S1. PEIS fitting data for the Flat-100 and Nanonet-100 samples

Sample		**Irradiation direction**	**Applied potential** (V_{RHE})							
			0.9	1	1.1	1.2	1.3	1.4	1.5	1.6
Flat-100	R_{SC}	Front	295	71.41	123.4	552.4	1241	1779	2319	2408
	(Ω)	Back	65.83	1121	278.1	297.5	261.7	303.6	357.1	396.6
	R_{CT}	Front	3714	1247	1838	6364	14370	14130	13030	9393
	(Ω)	Back	25460	44990	24070	5676	1362	774	597.1	621.8
Nanonet-100	R_{SC}	Front	325	217.4	129.8	122.6	130.2	143.7	162.5	180.6
	(Ω)	Back	3155	2685	1249	466.3	234.2	169.7	117.7	88.86
	R_{CT}	Front	18630	2753	467.6	171.7	131.2	142.2	169.8	210
	(Ω)	Back	63220	71150	43770	5899	992.9	711.9	605.4	371.1

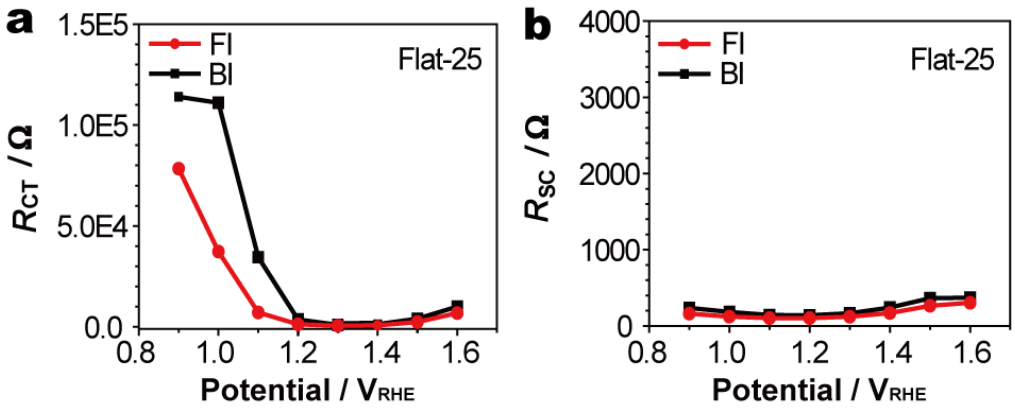

Figure S6. (a) The R_{CT} under frontside irradiation and backside irradiation of Flat-25; (b) The R_{SC} under frontside and backside irradiation of Flat-25.

Figure S6 shows that for the Flat-25 sample, both the surface charge transfer resistance (R_{CT}) and the bulk charge transfer resistances (R_{SC}) become larger at high applied potentials (> 1.3 V_{RHE}) regardless of the irradiation direction. This observation suggests the increased surface recombination at high applied potentials in the Flat-25 photoanode.

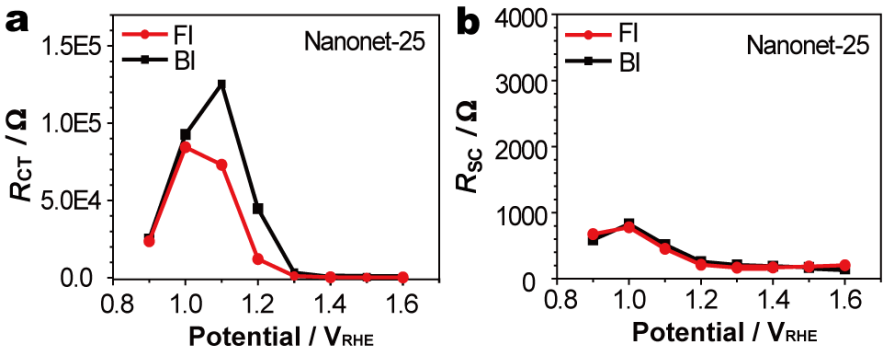

Figure S7. (a) The R_{CT} under frontside irradiation and backside irradiation of Nanonet-25; (b) The R_{SC} under frontside and backside irradiation of Nanonet-25.

Figure S7 shows that in the Nanonet-25 sample, the surface charge transfer resistance (R_{CT}) decreases with the increase of applied potentials when applied potentials > 1.1 V_{RHE} under both FI and BI, which is different from the increase on R_{CT} at high applied potentials in the Flat-25 sample. This observation suggests the nanonet structure can hinder the surface recombination in the Flat samples by promoting interfacial charge transfer at the SCLJ.

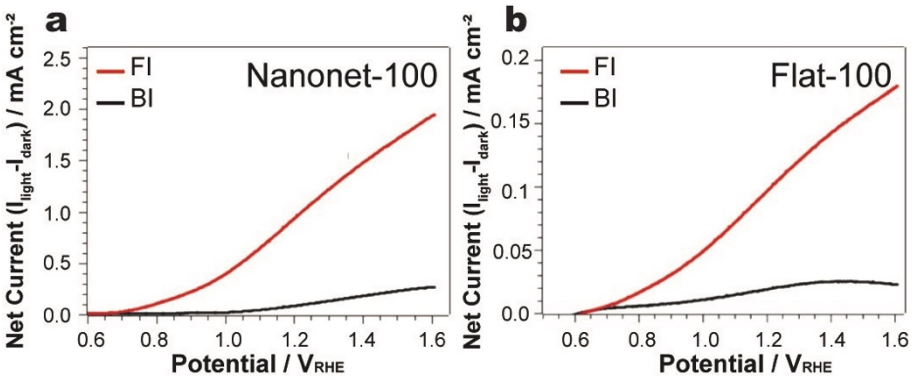

Figure S8. Net current of (a) Nanonet-100 and (b) Flat-100 under backside irradiation and frontside irradiation in hole sacrificial agent (0.5 M H_2O_2).

For both the Flat-100 and Nanonet-100 samples, the photocurrent density measured in the electrolyte with the H_2O_2 hole sacrificial agent under FI is always greater than that under BI, demonstrating that more photogenerated holes can actually transfer across the SCLJ.

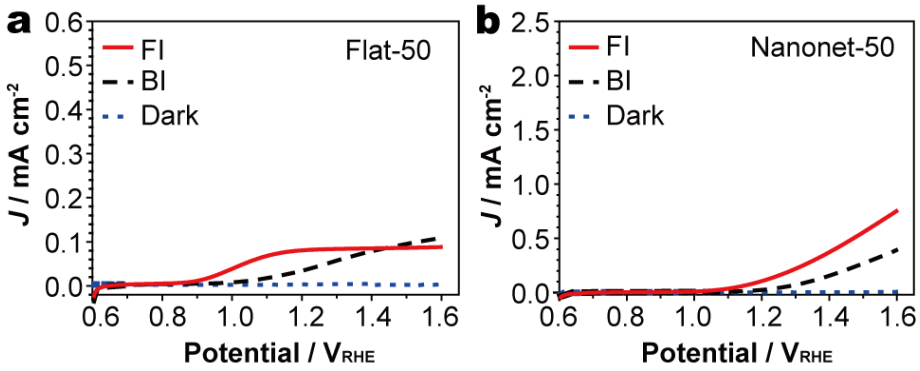

Figure S9. J-V curves in the dark, under backside irradiation and frontside irradiation of: (a) Flat-50 and (b) Nanonet-50.

Figure S9 shows that like the Flat-100 sample, the FI photocurrent is also overtook by the BI photocurrent at an applied bias higher than ca. 1.45 V_{RHE} for the Flat-50 sample, and also this abnormal phenomenon is avoided by patterning the planar surface with nanostructure as demonstrated in Nanonet-50.

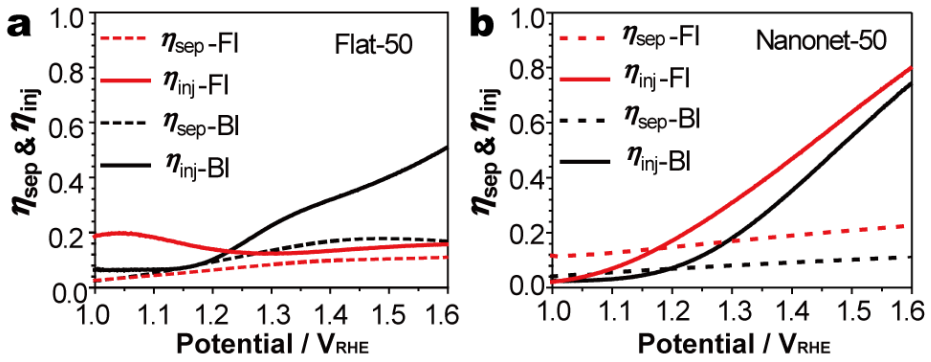

Figure S10. Charge injection efficiency (η_{inj}) and charge separation efficiency (η_{sep}) of (a) Flat-50 and (b) Nanonet-50 under frontside irradiation and backside irradiation.

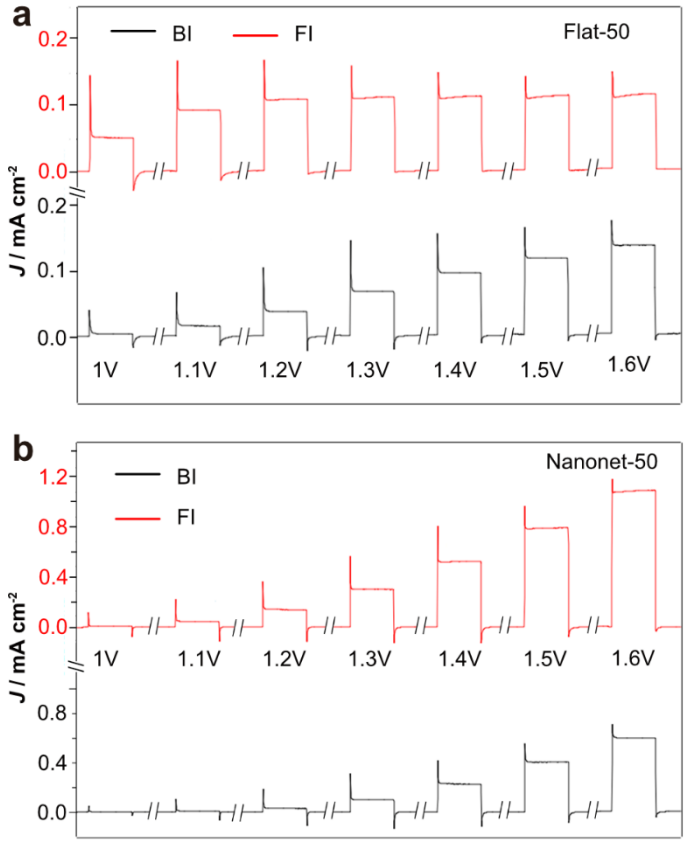

Figure S11. Transient photocurrent of (a) Flat-50 and (b) Nanonet-50 at different bias voltages under both frontside irradiation and backside irradiation.

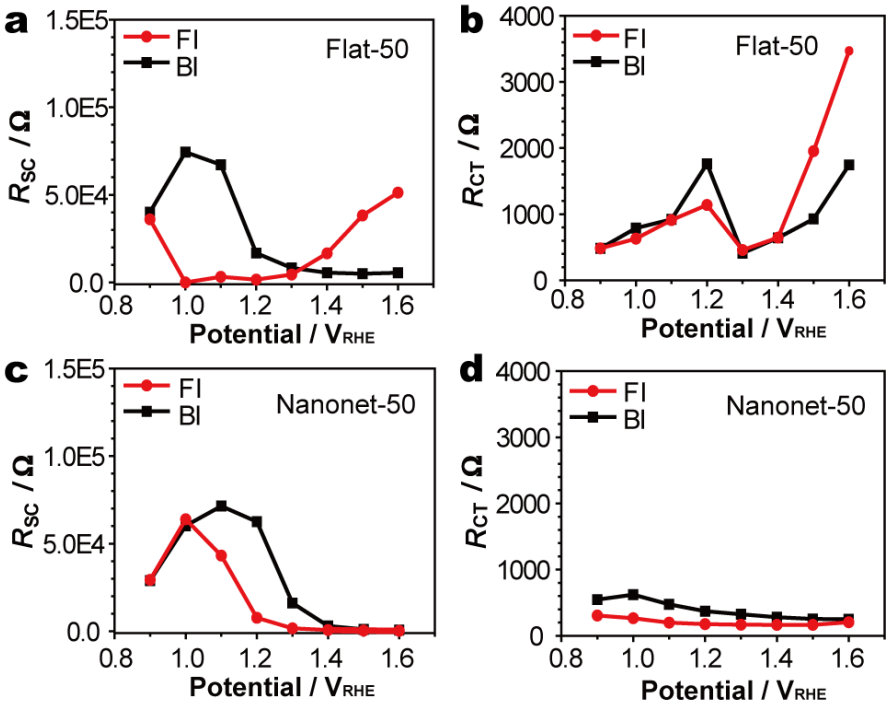

Figure S12. The R_{CT} under frontside irradiation and backside irradiation: (a) Flat-50, (c) Nanonet-50; The R_{SC} under frontside and backside irradiation: (b) Flat-50, (d) Nanonet-50.

Figure S10-S12 suggest the high surface recombination in the Flat-50 sample at high biases under FI, thus leading to the abnormal phenomenon that FI photocurrent is overtook by BI photocurrent at large bias range, which is also avoided in the Nanonet-50 sample because of the decreased surface recombination. These observations further support our conclusions drawn from the Flat-100 and Nanonet-100 samples.

References

[1] M. Szekeres, O. Kamalin, R. A. Schoonheydt, K. Wostyn, K. Clays, A. Persoons, I. Dékány, *J. Mater. Chem.* **2002**, *12*, 3268-3274.

[2] L. Zhang, E. Reisner, J. J. Baumberg, *Energy Environ. Sci.* **2014**, *7*, 1402-1408.

[3] I. Kondofersky, H. K. Dunn, A. Müller, B. Mandlmeier, J. M. Feckl, D. Fattakhova-Rohlfing, C. Scheu, L. M. Peter, T. Bein, *ACS Appl. Mater. Interfaces* **2015**, *7*, 4623-4630.

[4] M. Butler, *J. Appl. Phys.* **1977**, *48*, 1914-1920.

[5] T. Lopes, L. Andrade, F. Le Formal, M. Gratzel, K. Sivula, A. Mendes, *Phys. Chem. Chem. Phys.* **2014**, *16*, 16515-16523.